Journal of Sound and Vibration (1998) **210**(4), 461–481

STICK–SLIP–SEPARATION ANALYSIS AND NON-LINEAR STIFFNESS AND DAMPING CHARACTERIZATION OF FRICTION CONTACTS HAVING VARIABLE NORMAL LOAD

B. D. YANG, M. L. CHU AND C. H. MENQ

Coordinate Metrology and Measurement Laboratory, Department of Mechanical Engineering, The Ohio State University, Columbus, OH 43210, U.S.A.

(*Received* 15 *January* 1997, *and in final form* 5 *September* 1997)

Mechanical systems in which moving components are mutually constrained through contacts often lead to complex contact kinematics involving tangential and normal relative motions. A friction contact model is proposed to characterize this type of contact kinematics that imposes both friction non-linearity and intermittent separation non-linearity on the system. The stick–slip friction phenomenon is analyzed by establishing analytical criteria that predict the transition between stick, slip, and separation of the interface. The established analytical transition criteria are particularly important to the proposed friction contact model for the transition conditions of the contact kinematics are complicated by the effect of normal load variation and possible interface separation. With these transition criteria, the induced friction force on the contact plane and the variable normal load perpendicular to the contact plane can be predicted for any given cyclic relative motions at the contact interface and hysteresis loops can be produced so as to characterize the equivalent damping and stiffness of the friction contact. These non-linear damping and stiffness methods along with the harmonic balance method are then used to predict the resonant response of a frictionally constrained two-degree-of-freedom oscillator. The predicted results are compared with those of the time integration method and the damping effects, the resonant frequency shift, and the jump phenomenon are examined.

1. INTRODUCTION

When two vibrating bodies are mutually constrained through a friction contact, in the most general case, the relative motion of the two contacting surfaces is 3-D and can be resolved into two components: tangential component on the contact plane and normal component perpendicular to the plane (see Figure 1). The tangential component induces stick–slip friction, while the normal component causes normal load variation and possible intermittent separation of the contacting surfaces. The type of contact kinematics can occur in various mechanical systems, such as shroud contact interfaces of shrouded blade systems in turbine jet engines [1–3] and automotive clutches [4].

In the 3-D contact kinematics described above, the tangential motion that resides on the contact plane is 2-D in general; however, this work focuses on a simplified version of the 3-D contact kinematics, in which the contacting surfaces move with respect to each other back and forth along a straight line, while the normal component of the relative motion is retained. This simplified version is of interest because it can be regarded as the first step towards understanding the general case of contact kinematics.

When experiencing the contact kinematics having tangential and normal relative motion, the two vibrating bodies often exhibit complex dynamic behaviors due to the influence of

0022–460X/98/090461 + 21 $25.00/0/sv971305

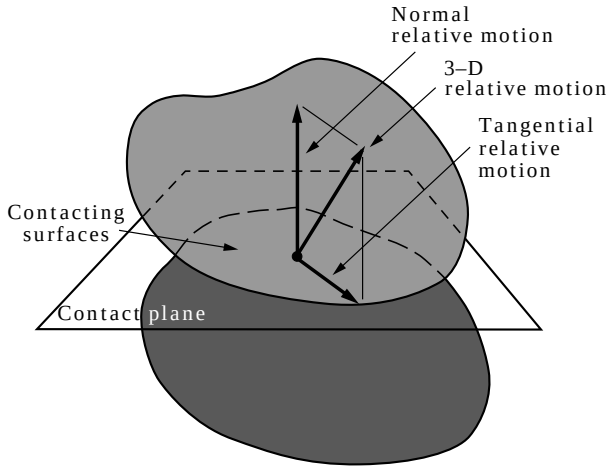

Figure 1. Contact kinematics.

friction and interface separation. Since both friction and interface separation are inherently non-linear phenomena, accurate predictions of the dynamic responses of the influenced structures require characterization of the non-linear contact kinematics with high fidelity. When the contact kinematics is simple and has negligible normal relative motion, the response of structures is only affected by the friction non-linearity, which can often be characterized by a friction interface model assuming constant normal load. This friction model often leads to a simple hysteresis loop that can be used to establish the damping and stiffness characteristics of the friction interface. The application of this simple friction interface model to friction damping design has received significant attention from a number of researchers [5–11]. On the other hand, when the normal relative motion of two neighboring structures is large, the structures may experience intermittent separation. This intermittent separation of the contact interface often gives rise to a non-linear stiffness characteristic that is amplitude-dependent. The intermittent separation non-linearity has been examined by a number of researchers under the frictionless condition [12–15]. The effect of motion-dependent normal load has been summarized by Ferri [16].

In this paper, a friction contact model is proposed to characterize the contact kinematics that imposes both friction non-linearity and intermittent separation non-linearity on the constrained structures. The stick–slip friction phenomenon is examined under the condition of variable contact normal load and interface separation. The contact kinematics is analyzed by establishing analytical criteria that predict the transition between stick, slip, and separation of the interface. The established analytical transition criteria are particularly important to the proposed friction contact model for the transition conditions of the contact kinematics are complicated by the effect of normal load variation and possible interface separation. With these transition criteria, the induced friction force on the contact plane and the variable normal load perpendicular to the contact plane can be predicted for any given cyclic relative motions at the contact interface and hysteresis loops can be produced so as to characterize the equivalent damping and stiffness of the friction contact. The non-linear damping and stiffness along with the harmonic balance method can be integrated together to obtain a set of non-linear algebraic equations, which can be solved iteratively for the resonant response [3]. However, the non-linear damping and stiffness can also be calculated from the friction force histories directly [17, 18]. In this work, the non-linear damping and stiffness along with the harmonic balance method are

used to predict the resonant response of a frictionally constrained two-degree-of-freedom (2DOF) oscillator. The predicted results are compared with those of the time integration method and the resulting damping effects the resonant frequency shift, and the jump phenomenon are examined. The application of the contact model to the prediction of the resonant response of shrouded blade systems and the design of shroud contact was reported in reference [3].

2. CONTACT INTERFACE MODEL

The contact interface between two vibrating bodies can be modelled as a substructure that contains a massless elastic element and a friction contact point, as depicted in Figure 2. The stiffness of the elastic element is characterized by two linear springs, k_u and k_v, which account for the shear and normal stiffness properties respectively. The friction contact point, that is assumed to obey the Coulomb friction law with the friction coefficient μ when in contact with *Body 2*, can undergo tangential stick–slip motion, and may experience intermittent separation from *Body 2* when the normal relative motion (v) becomes large. The contact interface is assumed to have either a preload or an initial gap (as designated by n_0). This model allows a negative preload to represent the situation when the interface has an initial gap; the equivalent preload across the interface with a gap e is calculated as $-k_v e$. In this model, u and v are the input tangential relative motion and normal relative motion of the contact interface respectively, and they can be evaluated as the motion of *Body 1* with respect to *Body 2* (that can be considered as the ground). The slip motion w is the tangential motion of the contact point relative to *Body 2*. The variable normal load n and the induced friction force f can be expressed as

$$n = \begin{cases} n_0 + k_v v, & \text{when } v \geqslant -n_0/k_v, \\ 0, & \text{when } v < -n_0/k_v, \end{cases} \tag{1}$$

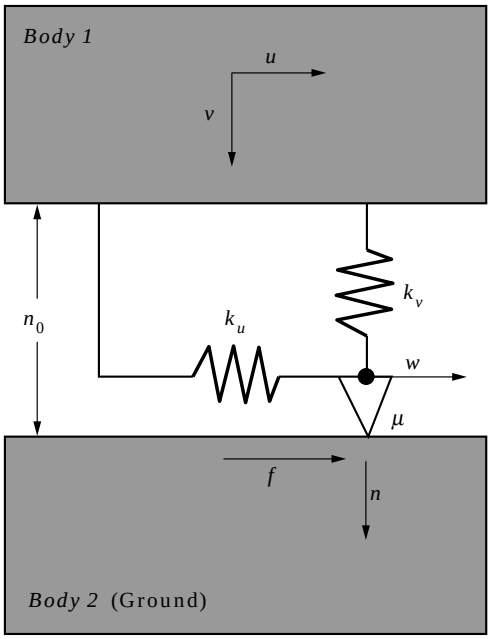

Figure 2. Contact interface model.

$$f = k_u(u - w). \tag{2}$$

It is noted that the normal load variation is proportional to the normal relative motion when the two bodies remain in contact.

2.1. STICK, SLIP, AND SEPARATION

When the vibratory motion is small, the contact surface sticks and the friction force is proportional to the tangential relative motion u with reference to w, which is zero. Its magnitude is always limited by the slip load $\pm\mu n$. During the course of vibration, the interface may reach a point where the friction force tends to exceed the positive slip load μn, and the contact surface starts to slip towards the positive u direction. Subsequently, the friction force remains equal to the varying slip load until the contact surface sticks again. Here, it should be pointed out that the moment when the interface changes back to the stick state does not correspond to when the tangential relative motion u reverses its direction. The reason is that the transition from slip to stick depends on the tangential relative motion u as well as the variable normal load, and in the process the normal load may decrease to reduce the slip load so that the occurrence of the transition can be postponed to some instant after the reversion of the motion u. When the interface moves towards the negative u direction, the interface repeats the process in the opposite direction. During the cycle of motion, the contact normal load may vanish and cause the interface to separate; consequently, the friction force is not present.

2.2. PRELOAD AND INITIAL GAP

Depending on the initial condition of the contact interface, the intermittent separation due to large normal relative motion can have two different types. When the interface is preloaded, small normal relative motion does not cause any separation but keeps the interface remaining in contact throughout the motion. As the amplitude of the normal relative motion increases, the temporary separation of the interface occurs when the motion approaches one of its extremes. On the other hand, when the interface has an initial gap, small normal relative motion does not cause any contact in the interface, resulting in a situation of fully separation throughout the motion. The increase in the amplitude of the normal relative motion causes the fully separation to be interrupted for some portion of the cyclic motion. It is evident that these two different types of intermittent separation can lead to different non-linear stiffness characteristics.

3. STICK–SLIP ANALYSIS

The simplest friction interface model is the one having constant normal load, as depicted in Figure 3, in which one of the two contact bodies is assumed to be the ground. When the interface is subjected to cyclic relative motion (say $u = A\cos\theta$, $\theta = \omega t$), it undergoes alternating stick–slip motion, and the resulting hysteresis loop consists of two symmetric stick regions and two symmetric slip regions, also shown in Figure 3 [8]. For an interface experiencing in-phase variable normal load,† as demonstrated by Menq *et al*. [2], the resulting hysteresis loop is shown in Figure 4, in which the slip regions become inclined lines because of the in-phase variable normal load that is taken as the sum of the preload, n_0, plus a term proportional to the tangential relative motion. In both hysteresis loops, the stick–slip transitions can be easily predicted. In particular, the slip-to-stick transitions

† The friction interface model assuming in-phase variable normal load is a special case of the interface model shown in Figure 2, in which the normal relative motion that causes the normal load variation is in phase with the tangential relative motion.

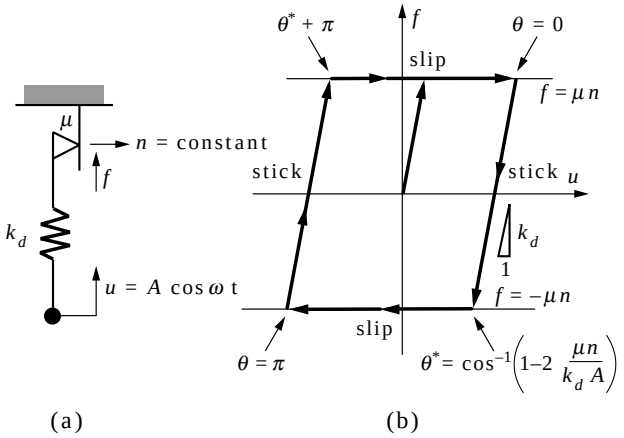

Figure 3. Hysteresis loop of an interface experiencing constant normal load: (a) friction interface model, (b) hysteresis loop.

always occur at the instant when the relative motion reverses its direction ($\theta = 0^\circ$ or $\theta = 180^\circ$).

On the other hand, when an interface experiences variable normal load whose variation has an arbitrary phase angle from the tangential relative motion, it becomes more difficult to predict the stick–slip transition. This is because the transition depends on not only tangential relative motion but also normal load variation. For example, the slip-to-stick transition may not occur when tangential relative motion reverses its direction; instead, variable normal load may decrease to keep the interface remaining slipping. To illustrate the complex friction phenomenon caused by normal load variation, one typical example of the hysteresis loop is shown in Figure 5. The hysteresis loop also consists of four alternating stick and slip regions, but it is more complicated than those of the case of constant normal load or of in-phase variable normal load. As can be seen in this complex hysteresis loop, the two slip-to-stick transitions do not occur at the moment of motion reversion that coresponds to $\theta = 0^\circ$ or $\theta = 180^\circ$. One transition takes place at some instant after the motion reverses its direction ($\theta_1 = 22{\cdot}9^\circ$), and the other transtion takes place at some instant before the motion reverses its direction ($\theta_3 = 159{\cdot}7^\circ$).

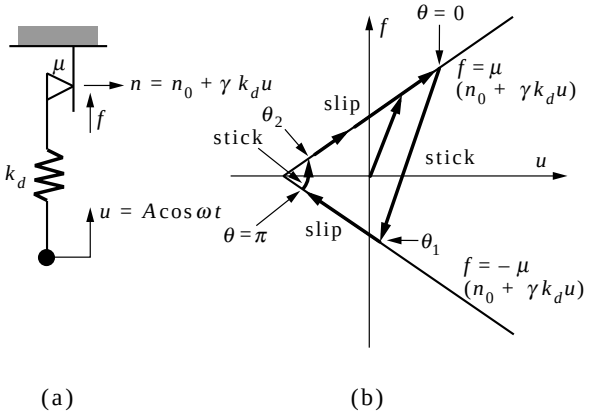

Figure 4. Hysteresis loop of an interface experiencing in-phase variable normal load: (a) friction interface model; (b) hysteresis loop. $\theta_1 = \cos^{-1}[(-2\mu n_0/k_d A - \mu\gamma + 1)/(1 - \mu\gamma)]$, $\theta_2 = \cos^{-1}[(2\mu n_0/k_d A - \mu\gamma - 1)/(1 - \mu\gamma)]$.

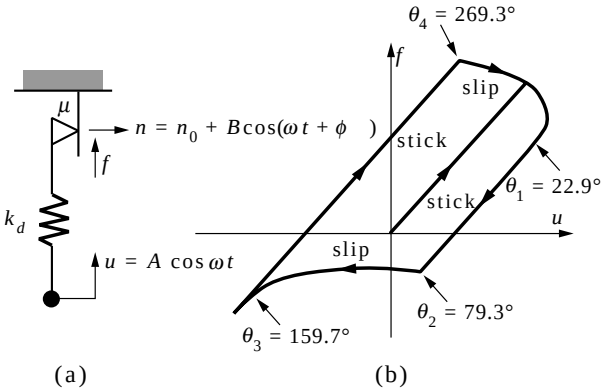

Figure 5. Typical hysteresis loop of an interface experiencing variable normal load: (a) friction interface model, (b) hysteresis loop.

In the following sections, the stick–slip analysis of a friction interface experiencing variable normal load will be presented. Using the proposed model shown in Figure 2, analytical criteria are developed to predict the transitions between various states of the interface (stick, slip, and separation). With the transitions established, the hysteresis loop can be extablished to characterize the stiffness and damping of the interface.

3.1. STICK–SLIP CHARACTERISTICS

To establish the transition criteria, the stick–slip condition must first be addressed in an analytical form. In other words, the friction force f and the slip velocity $\dot{w}$ that characterize the stick–slip condition must be formulated in terms of the input relative motion. These two quantities are referred to as the stick–slip characteristics of the friction interface. With these stick–slip characteristics determined, the criteria can then be established in terms of the input relative motion.

When the interface sticks, $\dot{w} = 0$, and from equation (2) the friction force can be given in the form

$$f = k_u(u - u_0) + f_0, \tag{3}$$

where u_0 and f_0 are the initial values of u and f at the beginning of the stick state.

When the positive slip occurs, the contact surface moves towards the positive direction; that is, $\dot{w} > 0$. In this state, the friction force is equal to the positive slip load:

$$f = \mu n. \tag{4}$$

Considering equation (1), it becomes

$$f = \mu n_0 + \mu k_v v. \tag{5}$$

The slip velocity $\dot{w}$ can be found in terms of the input relative motion by differentiating equations (1), (2) and (5) with respect to time and rearranging them:

$$\dot{w} = \dot{u} - \frac{\mu k_v}{k_u}\dot{v}. \tag{6}$$

Similarly, one can conclude the stick–slip characteristics for the negative slip state (when the contact surface moves towards the negative direction) as follows:

$$f = -(\mu n_0 + \mu k_v v), \qquad \dot{w} = \dot{u} + \frac{\mu k_v}{k_u}\dot{v}. \tag{7, 8}$$

3.2. TRANSITION CRITERIA

As indicated, the interface will be in one of the four distinct states: stick, positive slip, negative slip, and separation.

3.2.1. *Stick state*

When the interface sticks, the transitions to slip states occur when the friction force reaches the slip load:

$$\text{positive slip:} \qquad f - \mu n = 0, \qquad \dot{f} - \mu \dot{n} > 0; \tag{9}$$

$$\text{negative slip:} \qquad f + \mu n = 0, \qquad \dot{f} + \mu \dot{n} < 0. \tag{10}$$

The inequalities guarantee the slip conditions to be satisfied. Using equations (1) and (3), the above stick-to-slip transition criteria become

$$\text{positive slip:} \qquad k_u u - \mu k_v v + (f_0 - \mu n_0 - k_u u_0) = 0, \qquad k_u \dot{u} - \mu k_v \dot{v} > 0; \tag{11}$$

$$\text{negative slip:} \qquad k_u u + \mu k_v v + (f_0 + \mu n_0 - k_u u_0) = 0, \qquad k_u \dot{u} + \mu k_v \dot{v} < 0. \tag{12}$$

As for the stick-to-separation transition, it occurs when the normal load vanishes. Besides, the normal load must be decreasing at this moment to guarantee the occurrence of the separation. In other words, the criterion can be expressed as $n = 0$ and $\dot{n} < 0$. Using equation (1), it becomes

$$n_0 + k_v v = 0, \qquad \dot{v} < 0. \tag{13}$$

3.2.2. *Positive slip state*

Since the positive slip state cannot be followed by the negative slip state, only two transitions are possible. The transition to the stick state can be inferred from $\dot{w} = 0$ and $\ddot{w} < 0$; the latter one is required to ensure that the contact surface has a tendency towards the negative direction when it reaches the extreme. Using equation (6), these conditions imply

$$\dot{u} - \frac{\mu k_v}{k_u} \dot{v} = 0, \qquad \ddot{u} - \frac{\mu k_v}{k_u} \ddot{v} < 0. \tag{14}$$

It can be clearly seen that this slip-to-stick transition depends on the tangential relative motion and the normal relative motion (thus the normal load variation) as well. However, for the simplified case of the constant normal load ($\dot{v} = 0$) and of the in-phase variable normal load ($\dot{v} \propto \dot{u}$), the transition criterion becomes $\dot{u} = 0$, that is, when the motion u reverses its direction.

Since the occurrence of the separation state only depends on the variable normal load, the criterion for the transition from the positive slip state to the separation state is the same as the criterion given by equation (13).

3.2.3. *Negative slip state*

A similar procedure to that for the case of the positive slip can be used in this case. The transition to the stick state occurs when $\dot{w} = 0$ and $\ddot{w} > 0$, namely

$$\dot{u} + \frac{\mu k_v}{k_u} \dot{v} = 0, \qquad \ddot{u} + \frac{\mu k_v}{k_u} \ddot{v} > 0. \tag{15}$$

The transition to the separation state occurs when the criterion given by equation (13) is met.

3.2.4. *Separation state*

The separation of the interface ends when the normal load is about to develop, and hence the moment of this transition can be determined by $n = 0$ and $\dot{n} > 0$. Using equation (1), the criterion becomes

$$n_0 + k_v v = 0, \qquad \dot{v} > 0. \tag{16}$$

In addition to this transition moment, the state that follows the separation state has to be further determined. The stick–slip characteristics as shown in the previous section can be used to serve this purpose.

When the normal load and the friction force begin to develop at the end of the separation, from equations (1) and (2) their rates of change at this moment can be expressed as

$$\dot{n} = k_v \dot{v}, \qquad \dot{f} = k_u(\dot{u} - \dot{w}). \tag{17, 18}$$

If the interface becomes stuck after the separation, considering the stick–slip characteristics in the stick state, the following conditions must be satisfied:

$$-\mu\dot{n} < \dot{f} < \mu\dot{n} \qquad \text{and} \qquad \dot{w} = 0. \tag{19}$$

Then, considering equations (17) and (18), these conditions become

$$\frac{-\mu k_v}{k_u}\dot{v} < \dot{u} < \frac{\mu k_v}{k_u}\dot{v}. \tag{20}$$

Using similar arguments, one can conclude the condition for the coming positive slip state:

$$\dot{u} > \frac{\mu k_v}{k_u}\dot{v}, \tag{21}$$

and the condition for the coming negative slip state:

$$\dot{u} < -\frac{\mu k_v}{k_u}\dot{v}. \tag{22}$$

3.3. TRANSITION ANGLES OF CYCLIC MOTION

The above transition criteria are obtained without any assumption on the input relative motion; thus, it is true for any prescribed relative motion of the interface. However, when considering cyclic motion, these transition criteria can be used to derive the transition angles during a cycle of motion. Assume the cyclic motion to be sinusoidal, namely

$$u = a \sin\theta, \qquad v = b \sin(\theta + \phi), \tag{23, 24}$$

where $\theta = \omega t$, in which ω is the oscillating frequency and t is the time. The interface may experience, during a cycle of motion, a sequence of states; as a result, the hysteresis loop is segmented into the corresponding stick, positive slip, negative slip, and separation regions. Applying the criteria described in the preceding section, eight transition angles† can be formulated to characterize the possible transitions from one state to another during a cycle of motion. In the following discussion, the symbol E denotes the stick state, the symbol N the negative slip state, the symbol P the positive state, and the symbol S the separation state. The transition angle can be represented by ${}_{sub_l}\theta^{sup}_{sub_r}$, where the superscript

† For cyclic motion, the angle can be used to represent the dimensionless time, ωt. Since the damping and stiffness characteristics of a friction interface is independent of the frequency of the motion, the transition angle can be useful in this investigation.

represents the current state, the right subscript (sub_r) the following state, the left subscript (sub_l) the previous state.

The eight transition angles are listed as follows. ${}_N\theta_P^E$: Transition angle from the stick state to the positive slip state; the stick state follows the negative slip state. ${}_P\theta_N^E$: Transition angle from the stick state to the negative slip state; the stick state follows the positive slip state. ${}_S\theta_P^E$: Transition angle from the stick state to the positive slip state; the stick state follows the separation state. ${}_S\theta_N^E$: Transition angle from the stick state to the negative slip state; the stick state follows the separation state. θ_S^*: Transition angle from the stick, positive slip, or negative slip state to the separation state. θ_*^S: Transition angle from the separation state to the stick, positive slip, or negative slip state. θ_E^P: Transition angle from the positive state to the stick state. θ_E^N: Transition angle from the negative state to the stick state.

The formulas of these transition angles are given in the Appendix. From the formulas, it is clear that the first four transition angles are dependent on the previous state. However, the last four angles are independent of the previous state, and thus, the left subscript is neglected. It is noted that the interface separates during the period from θ_S^* to θ_*^S. These transition angles are expressed in terms of three dimensionless variables, namely $\bar{n}_0 = \mu n_0/k_u a$, $\overline{b} = \mu k_v b/k_u a$, and ϕ, and can be calculated in advance so as to construct the sequence of stick/slip/separation regions. Once the sequence of stick/slip/separation regions is known, the hysteresis loop can be established.

3.4. HYSTERESIS LOOP

It is found that there are 12 possible sequences of stick/slip/separation regions due to sinusoidal motion. They can be further categorized into three cases: no slip, slip but no separation, separation.

3.4.1. *No-slip case*

When the interface is held by the preload and the input relative motion is small, the interface sticks all the time. This case containing only the stick region occurs when

$$\bar{n}_0 > \frac{\sqrt{1+\overline{b}^2-2\overline{b}\cos\phi}+\sqrt{1+\overline{b}^2+2\overline{b}\cos\phi}}{2}. \tag{25}$$

This range of n_0 can be obtained by considering the condition that makes ${}_N\theta_P^E$ and ${}_P\theta_N^E$ non-existent, whose formulations can be found in the Appendix. Since the interface always sticks, it cannot contribute any damping to the system. Therefore, the relative motion and the induced friction force do not form a hysteresis loop.

3.4.2. *Slip-but-no-separation case*

When the amplitude of the relative motion increases to some extent, the interface begins to slip but still remains in contact. In this situation, the interface undergoes alternating stick–slip motion, which results in a hysteresis loop consisting of four alternating stick and slip regions separated by four transition angles, in the following order:

$$\theta_E^P \overset{E}{\rightarrow} {}_P\theta_N^E \overset{N}{\rightarrow} \theta_E^N \overset{E}{\rightarrow} {}_P\theta_N^E \overset{P}{\rightarrow} \theta_E^P.$$

Above the arrows are the corresponding regions between the two transition angles. This case occurs when

$$\frac{\sqrt{1+\overline{b}^2-2\overline{b}\cos\phi}+\sqrt{1+\overline{b}^2+2\overline{b}\cos\phi}}{2} > \bar{n}_0 > \overline{b}. \tag{26}$$

It is apparent that the shape of the resulting hysteresis loop changes as the phase angle (ϕ) between u and v changes. This variation with changing the phase angle is depicted in Figure 6, in which $k_u = k_v = 1$, $\mu = 0{\cdot}4$, $n_0 = 1{\cdot}2$, $a = b = 1$, and the phase angle for each loop is shown alongside.

Since the analytical transition criteria are developed for the general variable normal load case, they can also be applied to its simplified cases of constant normal load and in-phase variable normal load. This can be illustrated by the resulting hysteresis loop shown in Figure 6 for the in-phase variable normal load case ($\phi = 0^\circ$). It is apparent that this hysteresis loop is so simple that these transitions can be easily determined, even without the help of the developed transition criteria. For example, the slip-to-stick transitions (θ_E^P and θ_E^N) occur as the motion reverses the direction. However, when the phase angle is present, the slip-to-stick transitions do not take place at the moment of motion reversion.

3.4.3. *Separation case*

When the normal relative motion becomes larger and larger, the interface that is initially held by a preload will separate for a while during a cycle of motion. On the other hand, when the interface has an initial gap and is subjected to a sufficiently large normal relative motion, the gap will be closed for a portion of the cycle. There exist 10 possible sequences of stick/slip/separation regions and they are listed in Figure 7. This tree-type scheme starts from the separation region, after which a three-way branch indicates the possibility of the stick, positive slip, or negative slip region. The decision can be made based on the criteria given by equations (20)–(22). In addition to this particular branch, there are seven two-way branches whose decisions have to be made between two transition angles. For example, the positive slip region that follows the separation region may change to the stick region

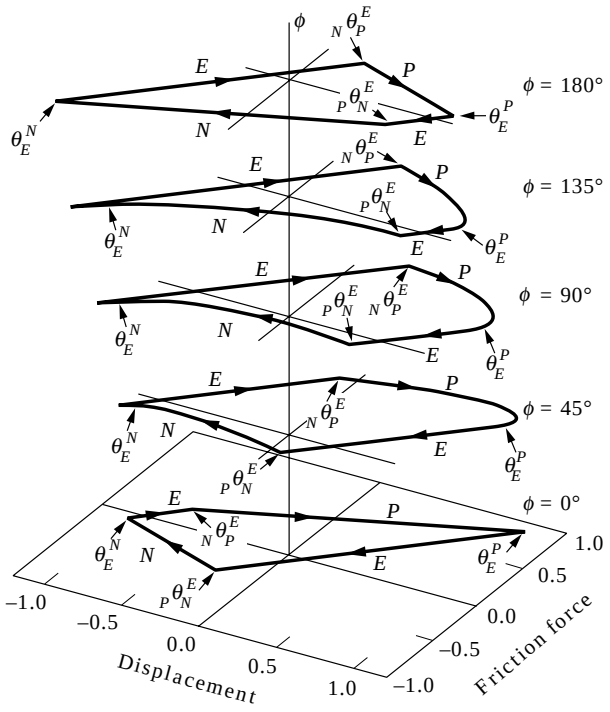

Figure 6. Variation in hysteresis loop (slip-but-no-separation).

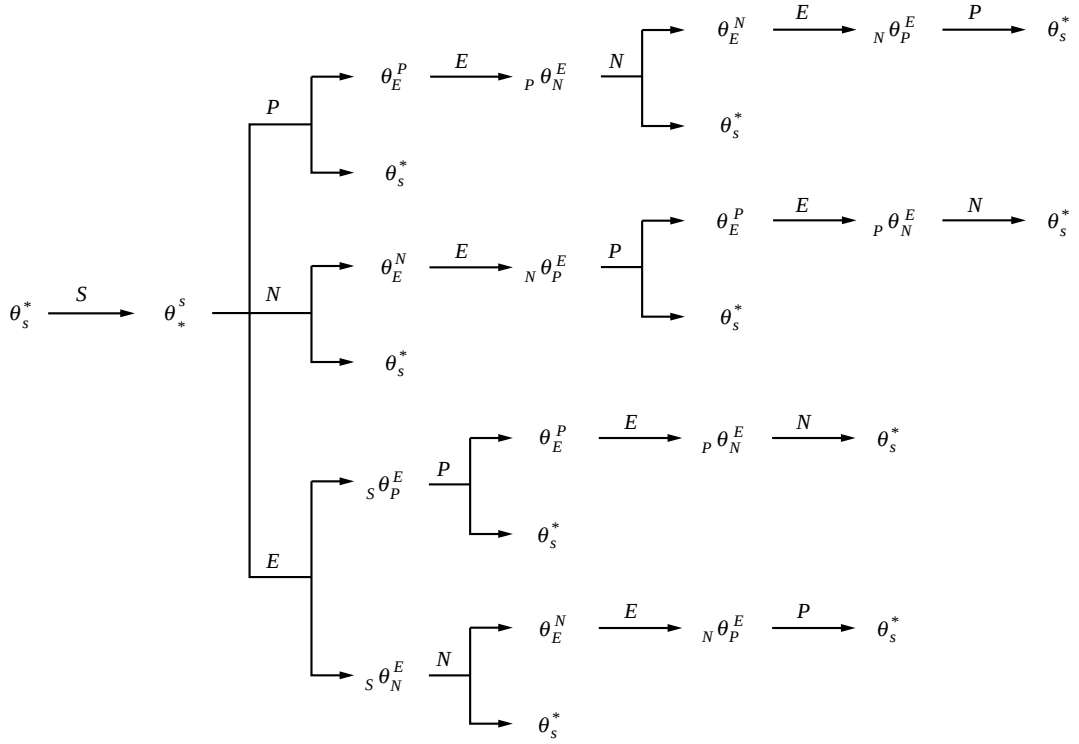

Figure 7. Ten possible sequences of regions in the separation case.

at the transition angle θ_E^p or back to the separation region at the transition angle θ_S^*. Since the transition angles are calculated in advance, the decision can be made based on which angle is first encountered.

The occurrence of the intermittent separation complicates the stick–slip friction phenomenon, and thus, the resulting hysteresis loop becomes complex. In addition, the shape of the hysteresis loop may have significant variation due to the phase angle. This variation is depicted in Figure 8, in which the interface parameters and the relative motion are the same as those in the slip-but-no-separation case, except $n_0 = 0{\cdot}8$.

4. NON-LINEAR STIFFNESS AND DAMPING CHARACTERISTICS

Once the hysteresis loop of the friction contact interface is established by applying the stick–slip analysis discussed above, Fourier series expansion can be used to lump the induced friction force into the equivalent stiffness and damping terms. These lumping effects along with the effect of the intermittent separation caused by normal relative motion can be integrated with the harmonic balance method to predict the forced response of frictionally constrained structures.

4.1. FRICTION FORCE

For input harmonic relative motion, as expressed in equations (23) and (24), the induced periodic friction force can be approximated by

$$f(\theta) \approx k_u a(F_b(\bar{n}_0, \bar{b}, \phi) + F_s(\bar{n}_0, \bar{b}, \phi) \sin\theta + F_c(\bar{n}_0, \bar{b}, \phi) \cos\theta), \tag{27}$$

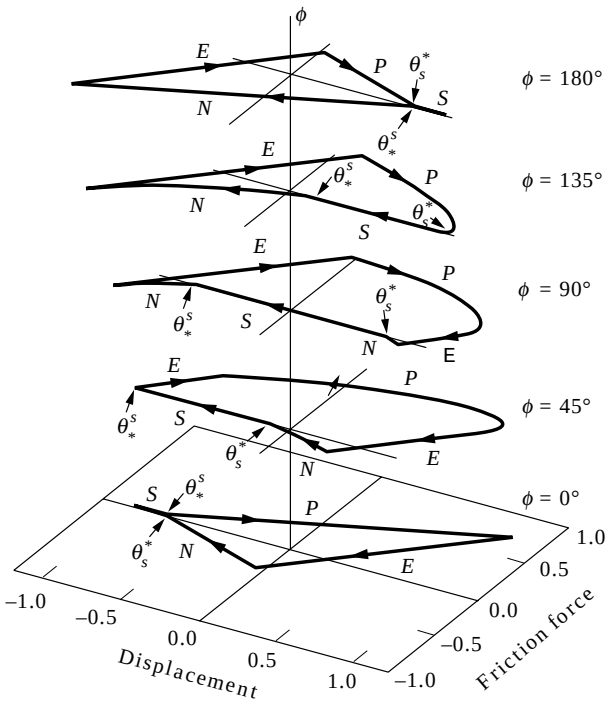

Figure 8. Variation in hysteresis loop (separation).

where F_b, F_s, and F_c are the three non-dimensionalized Fourier coefficients, and they are the functions of the three dimensionless variables, $\bar{n}_0 = \mu n_0/k_u a$, $\overline{b} = \mu k_v b/k_u a$, and ϕ. These three Fourier coefficients represent three important components of the induced friction force. The time invariant component, $k_u a F_b$, is important for it can result in static deflection of the constrained structures, and when dealing with complex structures, such as shrouded blades, the static deflection may cause an additional component of the contact preload, which can alter the induced friction force. The second term, $k_u a F_s$, represents the component of the friction force that is in phase with the tangential motion, therefore, F_s is the non-dimensionalized equivalent stiffness of the friction contact on the contact plane. On the other hand, F_c is related to the equivalent damping of the friction contact on the contact plane, because $k_u a F_c$ represents the component of the friction force that is out of phase by 90° with the tangential motion. The estimation of the stiffness and damping of the friction force using Fourier series expansion can be illustrated by Figure 9.

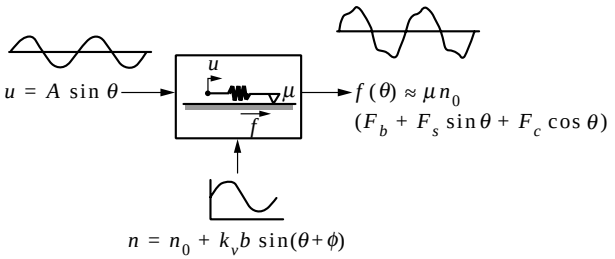

Figure 9. Estimation of stiffness and damping using Fourier series expansion.

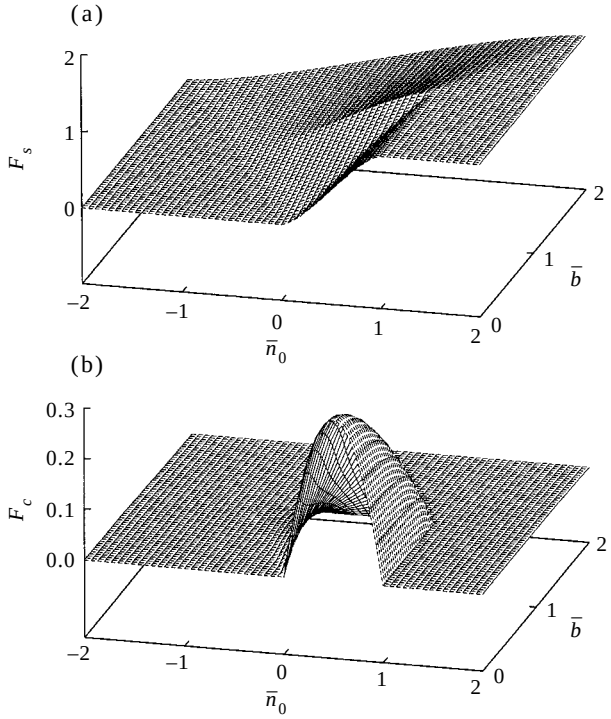

Figure 10. Non-dimensionalized stiffness and damping ($\phi = 0^\circ$): (a) stiffness F_s, (b) damping F_c.

By assigning a value to the phase angle (ϕ), these dimensionless Fourier coefficients will be functions of $\bar{n}_0$ and $\bar{b}$, which can be visualized as 3-D surfaces. Figure 10 depicts the two Fourier coefficients, F_s and F_c, for the case having $\phi = 0^\circ$. This is the in-phase case, which was studied by Menq *et al*. [2]. The boundary curves corresponding to $\bar{b} = 0$ in the two graphs are the results for the case having constant normal load, which was studied by a number of researchers [5, 8, 9]. It is interesting to note that, for the case of $\phi = 0^\circ$, the damping F_c is zero for the range of $\bar{b} > 1$. This is because the interface either separates or sticks during a cycle of motion, and thus, the hysteresis loop does not exist. The stick condition after separation can be inferred from equation (20). However, this is not the case when the phase angle ϕ exists. As shown in Figure 11, one can observe significant damping for the range of $\bar{b} > 1$. This indicates that the phase angle can have profound influence on the damping characteristic of the interface.

When a contact interface is subjected to large cyclic normal relative motion, the contact surfaces may separate intermittently. For the model shown in Figure 2, the variable contact normal load caused by harmonic normal relative motion, say $v = b \sin\theta$, can be expressed as

$$n = \begin{cases} n_0 + k_v b \sin\theta, & \text{when } \sin\theta \geqslant -n_0/k_v b, \\ 0, & \text{when } \sin\theta < -n_0/k_v b. \end{cases} \tag{28}$$

Since the variable normal load cannot contribute damping to systems, it must be in phase with the input normal relative motion and may be approximated by truncating the superharmonic terms in its Fourier series:

$$n \approx k_v b(N_b(n_0^*) + N_s(n_0^*) \sin\theta), \tag{29}$$

where n_0^* is the non-dimensionalized preload/gap, $n_0/k_r b$, and N_b and N_s are the non-dimensionalized Fourier coefficients of the time invariant term and the first fundamental terms, respectively. The time invariant component arises from the asymmetric nature of the intermittent separation, and it is important when the dynamic behavior of the constrained structure is examined. This is because the time invariant term alters the preload (or initial gap) of the contact interface and thus alters the response of the structure as well. Using the standard integral formula for the Fourier coefficient, the dimensionless functions N_b and N_s can be derived:

$$N_b(n_0^*) = \begin{cases} 0, & n_0^* < -1, \\ n_0^*, & n_0^* > 1, \\ (\sin\theta_1 + n_0^*\theta_1)/\pi, & |n_0^*| \leqslant 1; \end{cases} \tag{30}$$

$$N_s(n_0^*) = \begin{cases} 0, & n_0^* < -1, \\ 1 & n_0^* > 1, \\ (n_0^* \sin\theta_1 + \theta_1)/\pi, & |n_0^*| \leqslant 1; \end{cases} \tag{31}$$

in which $\theta_1 = \cos^{-1}(-n_0^*)$.

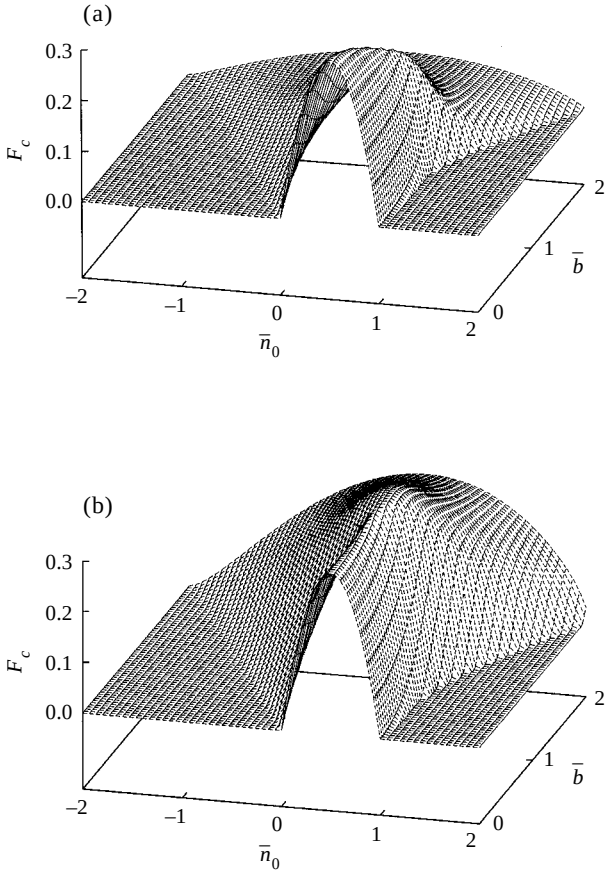

Figure 11. Non-dimensionalized damping: (a) $\phi = 15^\circ$, (b) $\phi = 30^\circ$.

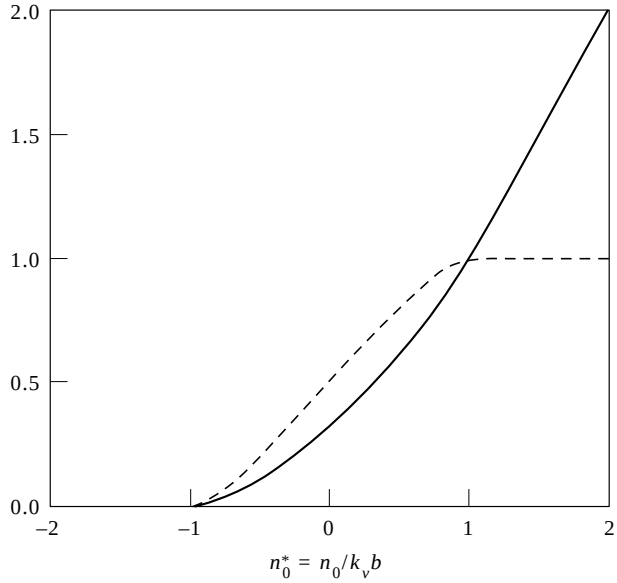

Figure 12. Non-dimensionalized Fourier coefficients of variable normal load: —, N_b; ---, N_s.

It is interesting to note that, depending on the initial interface condition, the non-linear stiffness nature, that is characterized by N_s, varies. This non-dimensionalized stiffness is illustrated in Figure 12. When the interface has preload and the relative normal motion is small such that $n_0^* > 1$, the contact interface does not separate throughout the motion and the non-dimensionalized stiffness is unity. As the relative normal motion becomes larger such that $n_0^* < 1$, the non-dimensionalized stiffness decreases and approaches 0·5, showing a "softening spring" characteristic.

For the case of having an initial gap, the contact interface does not exhibit any stiffness when the relative normal motion is small such that $n_0^* < -1$. This is because the gap never closes during a cycle of motion. As the relative normal motion becomes larger such that $n_0^* > -1$, the non-dimensionalized stiffness increases and approaches to 0·5, showing a "hardening spring" characteristic.

4.3. NON-LINEAR RESPONSE

The forced response of a two-degree-of-freedom oscillator under the contact constraint was investigated by the authors using the harmonic balance method in conjunction with the developed contact interface model [3]. Instead of using the conventional mass–spring–dashpot notation, this system can be described by its two-mode modal information that includes modal masses, $m_1 = 1{\cdot}0$, $m_2 = 1{\cdot}0$; modal frequencies, $\omega_{n1} = 1{\cdot}0$, $\omega_{n2} = 10{\cdot}0$; modal damping ratio, $\zeta_1 = 0{\cdot}01$, $\zeta_2 = 0{\cdot}01$; and mode shapes, $\Phi_1 = [0{\cdot}707 \;\; 0{\cdot}707]^T$, $\Phi_2 = [1{\cdot}0 \;\; -0{\cdot}5]^T$. As for the friction contact, the friction coefficient μ is 0·4, the shear stiffness k_u is 1·0, and the normal stiffness k_v is 1·0. Also, the external harmonic excitation can be broken into f_u, $f_u = 1{\cdot}0$, in shear direction, and f_v, $f_v = 1{\cdot}0$, in normal direction. The typical forced responses under various levels of preload are shown in Figure 13, in which the peak resonances are located within those of two lightly damped responses. The one for the fully separate case is the response of the oscillator without any influence of the interface, and the one for the fully stuck case is the response when the interface is totally locked up. Both are linear cases, but in between the problem becomes

non-linear due to the occurrence of friction slip and intermittent separation. In the figure, the discrete data points denote the results by the time integration method and they are used to verify the accuracy of the proposed approach. As expected, the damped resonant response, the resonant frequency shift, and the jump phenomenon are observed as the result of the coupling effect of these two non-linearities. The optimal preload $n_0 = 10$, which gives the minimum response, has an important implication to the design of friction contact in that it gives the most effective design when using the friction interface to attenuate the resonant response.

4.4. JUMP PHENOMENON

It is well known that the softening and hardening spring effects can lead to a jump phenomenon that indicates the possibility of multiple states in the response of the system within some frequency range. In Figure 13, for the case when the interface has a moderate initial gap ($n_0 = -20$), the contact of the two surfaces imposes a hardening spring effect on the structure to cause the resonance peak of the response to bend towards higher frequencies. On the other hand, for the case when the moderate preload is applied to the interface ($n_0 = 5$), the increase in the amplitude of the motion causes the preloaded interface to separate temporarily. The overall effect of the temporary separation is a

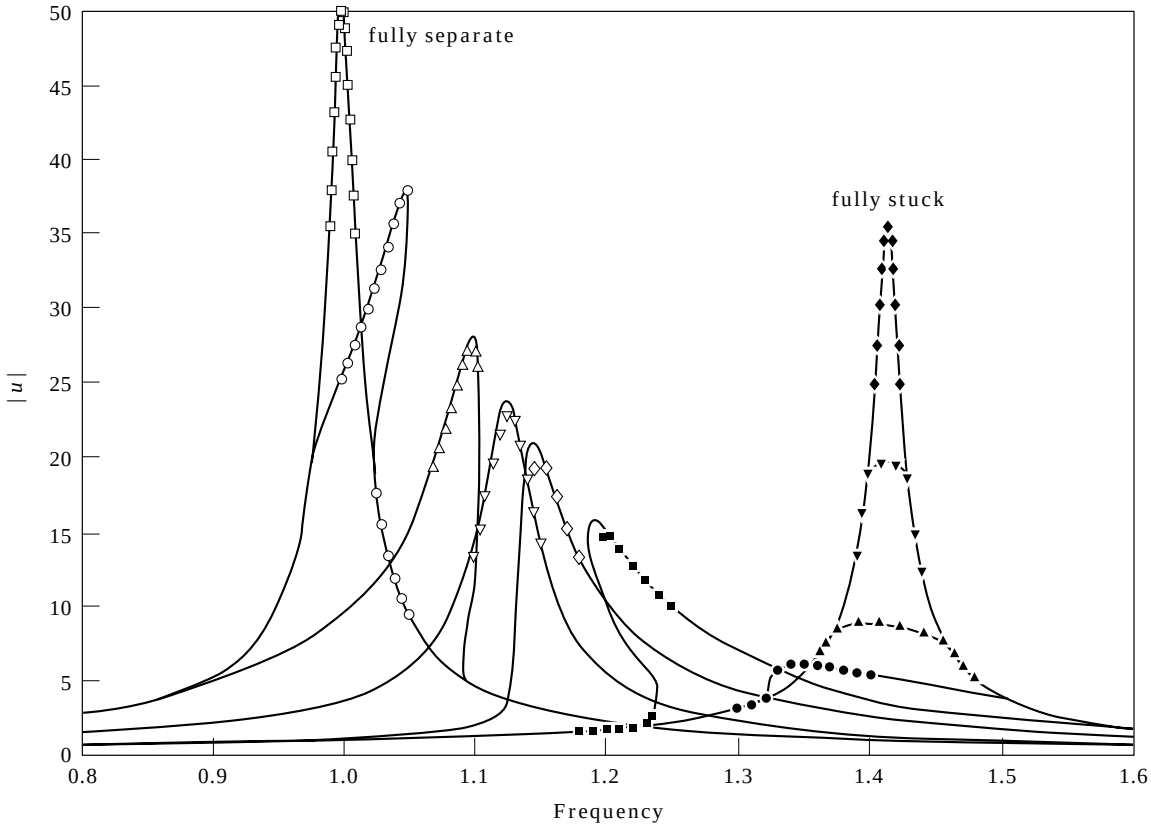

Figure 13. Forced responses of a two-degree-of-freedom oscillator: —, harmonic balance method. Discrete data, time integration method, n_0 values as follows: ◆, >90; ▼, 50; ▲, 20; ●, 10; ■, 5; ◇, 2; ∨, 0; ∧, -5; ○, -20; □, < -50.

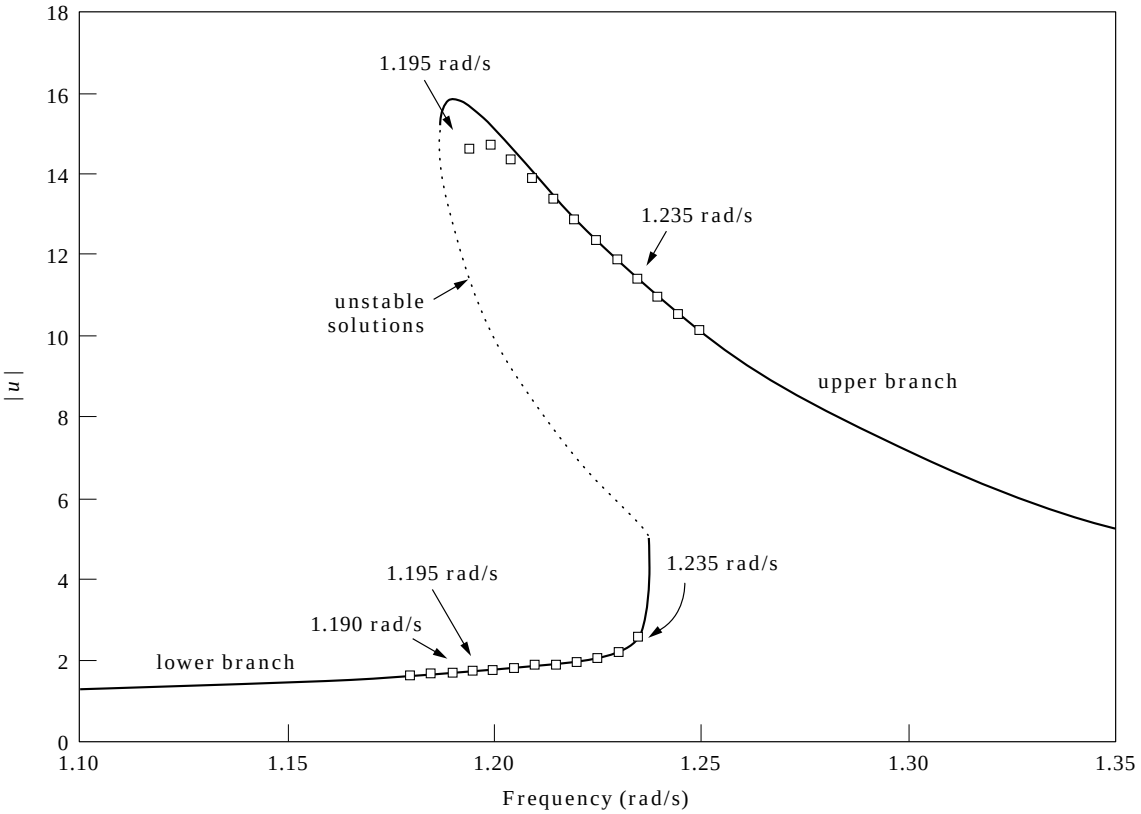

Figure 14. Response of the oscillator at $n_0 = 5$; —, harmonic balance method; □, time integration method; . . . . . , unstable solutions.

softening spring effect that gives rise to the non-linear response with a resonance peak bending towards lower frequencies.

To further examine the jump phenomenon, the direct time integration method is employed for the case of $n_0 = 5$ and the result is shown in Figure 14. For comparison, the solution from the harmonic balance method is also plotted in this figure. A slight discrepancy between these two solutions near the resonance can be observed. This is mainly due to the dissimilar effects of stick–slip friction and intermittent separation on the response of the oscillator that cause the assumption of the harmonic balance method regarding the harmonic nature of the motion to be not entirely accurate [19].

It should also be noted that one of the multiple solutions from the harmonic balance method shown as the dashed curve is unstable [20]; separated by the unstable response, the stable response consists of two curves, referred to as the upper and lower branches. The multiple solutions from the time integration method can be obtained by using different initial conditions; however, the unstable solutions cannot be reached because they are unstable. From the time integration solutions, the multi-valued response exists between 1·195 and 1·235 rad/s.

The "jumping" behavior can be clearly seen using the time integration simulation with frequency sweeping across the jump. The simulation starts from the frequency 1·195 rad/s for 100 cycles (phase I), is then perturbed to 1·190 rad/s for 120 cycles (phase II), and finally is perturbed back to 1·195 rad/s for 30 cycles (phase III). The result is shown in Figure 15. With the selected initial condition, the displacement at the end of phase I reaches the steady

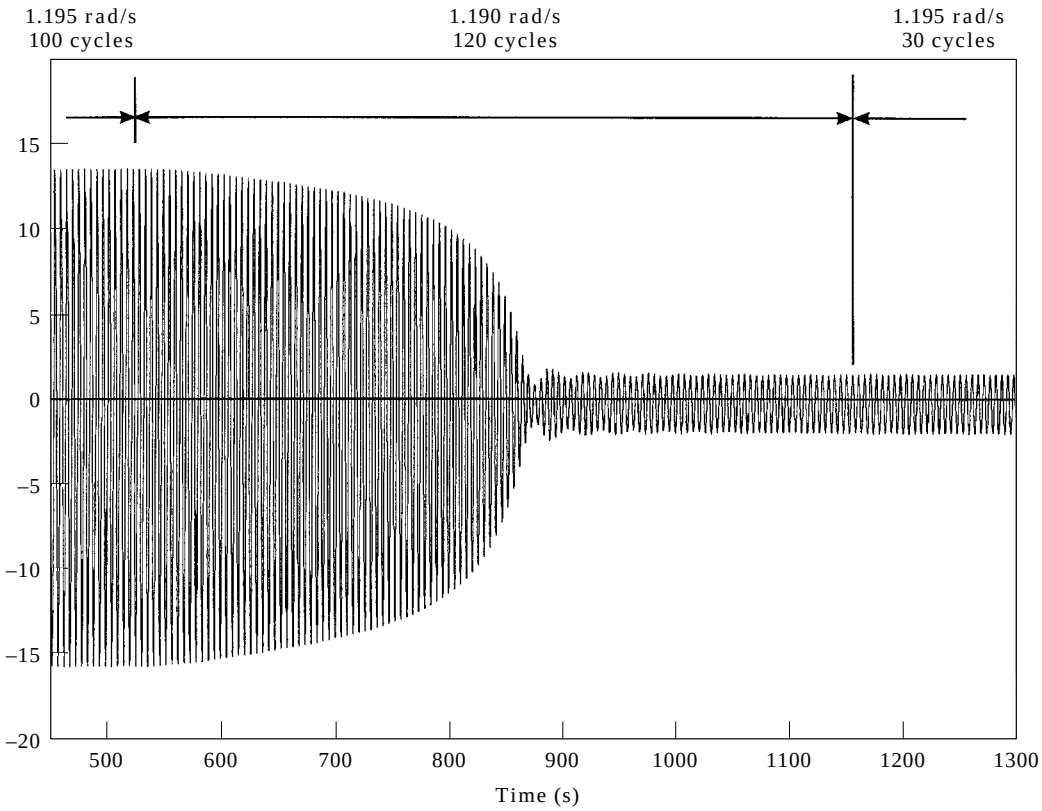

Figure 15. Time simulation of jump phenomenon.

state amplitude at the upper branch. In phase II, the steady state amplitude is reached after a transient period and jumps from the upper branch to the lower branch. In phase III, while the frequency is perturbed back to that of phase I, the steady state amplitude still stays in the lower branch.

5. CONCLUSIONS

A friction contact model has been proposed to characterize the contact kinematics that imposes both friction non-linearity and intermittent separation non-linearity on the constrained structures. In the stick–slip analysis, this interface model takes into account the variable normal load and possible interface separation caused by the normal relative motion. These effects can lead to a complex contact kinematics, in which the determination of the transition between various states of the interface (stick, slip, and separation) is not straightforward. In this study, the contact kinematics is analyzed by establishing analytical criteria that predict the transition between stick, slip, and separation of the interface. With these transition criteria, the induced friction force on the contact plane and the variable normal load perpendicular to the contact plane can be predicted for any given cyclic relative motions at the contact interface and hysteresis loops can be produced so as to characterize the equivalent damping and stiffness of the friction contact. The non-linear damping and stiffness along with the harmonic balance method are then used to predict the resonant response of a frictionally constrained two-degree-of-freedom oscillator. The

predicted results are compared with those of the time integration method and the resulting damping effect, the resonant frequency shift, and the jump phenomenon are examined.

Two types of intermittent separation of the interface caused by large normal relative motion were discussed. The first type occurs when the preloaded interface is subjected to large normal relative motion that causes the contact surfaces to separate temporarily during each cycle of motion. This type of intermittent separation can impose a softening spring effect on constrained structures. The second type of intermittent separation occurs when the normal relative motion becomes large and causes the interface having an initial gap to close for some portion of each cycle of motion. The effect of this type of intermittent separation is similar to the effect of a hardening spring.

The softening and hardening spring effects can lead to two stable frequency responses over some frequency range that cause the frequency response of the structure to have a jump phenomenon. The jumping behavior of the oscillator was studied using the time integration simulation with frequency sweeping across the jump. It was found that small perturbation in the excitation frequency near the jump of the response may cause the response to "jump" from one stable state to the other.

ACKNOWLEDGMENT

This material is based on work supported by the GUIde Consortium and the U.S. Air Force under contract No. F33615-92-C-2212. Any opinions, findings, and conclusions or recommendations expressed in this material are those of the authors and do not necessarily reflect the views of the GUIde Consortium or the Air Force.

REFERENCES

1. C. H. Menq, J. H. Griffin and J. Bielak 1986 *Transactions of the American Society of Mechanical Engineers*, *Journal of Vibration*, *Acoustics*, *Stress*, *and Reliability in Design* **108**, 50–55. The forced response of shrouded fan stages.
2. C. H. Menq, J. H. Griffin and J. Bielak 1986 *Transactions of the American Society of Mechanical Engineers*, *Journal of Engineering for Gas Turbines and Power* **108**, 300–305. The influence of a variable normal load on the forced vibration of a frictionally damped structure.
3. B. D. Yang and C. H. Menq 1996 *Transactions of the American Society of Mechanical Engineers*, *Journal of Engineering for Gas Turbines and Power* **119,** 958–963. Modeling of friction contact and its application to the design of shroud contact.
4. C. Padmanabhan 1994 *PhD Dissertation*, *The Ohio State University*. Analysis of periodically excited systems with clearances.
5. T. M. Cameron, J. H. Griffin, R. E. Kielb and T. M. Hoosac 1990 *Transactions of the American Society of Mechanical Engineers*, *Journal of Vibration*, *Acoustics*, *Stress*, *and Reliability in Design* **112**, 175–182. An integrated approach for friction damper design.
6. E. H. Dowell and H. B. Schwartz 1983 *Journal of Sound and Vibration* **91**, 255–267. Forced response of a cantilever beam with a dry friction damper attached, part I: theory.
7. E. H. Dowell and H. B. Schwartz 1983 *Journal of Sound and Vibration* **91**, 269–291. Forced response of a cantilever beam with a dry friction damper attached, part II: experiment.
8. J. H. Griffin 1980 *Transactions of the American Society of Mechanical Engineers*, *Journal of Engineering for Power* **102**, 329–333. Friction damping of resonant stresses in gas turbine engine airfoils.
9. C. H. Menq and J. H. Griffin 1985 *Transactions of the American Society of Mechanical Engineers*, *Journal of Vibration*, *Acoustics*, *Stress*, *and Reliability in Design* **107**, 19–25. A comparison of transient and steady state finite element analyses of the forced response of a frictionally damped beam.
10. A. V. Srinivasan and D. G. Cutts 1983 *Transactions of the American Society of Mechanical Engineers*, *Journal of Engineering for Power* **105**, 332–341. Dry friction damping mechanisms in engine blades.

11. E. J. Williams and S. W. Earles 1974 *Transactions of the American Society of Mechanical Engineers*, *Journal of Engineering for Industry* **96**, 471–476. Optimzation of the response of frictionally damped beam type structures with reference to gas turbine compressor blading.
12. S. Dubowsky and F. Freudenstein 1971 *Transactions of the American Society of Mechanical Engineers*, *Journal of Engineering Industry* **93**, 305–309. Dynamic analysis of mechanical systems with clearances, part I: formation of dynamic model.
13. S. Dubowsky and F. Freudenstein 1971 *Transactions of the American Society of Mechanical Engineers*, *Journal of Engineering Industry* **93**, 310–316. Dynamic analysis of mechanical systems with clearances, part II: dynamic response.
14. S. W. Shaw and P. J. Holmes 1983 *Journal of Sound and Vibration* **90**, 129–155. A periodically forced piecewise linear oscillator.
15. G. R. Tomlinson and J. Lam 1984 *Journal of Sound and Vibration* **96**, 111–125. Frequency response characteristics of structures with single and multiple clearance-type non-linearity.
16. A. A. Ferri 1996 *Transactions of the American Society of Mechanical Engineers*, *Journal of Vibration and Acoustics* **117**(B), 196–206. Friction damping and isolation systems.
17. J. Guillen and C. Pierre 1996 *Proceedings of the 1996 ASME IMECE*, *Atlanta*, *GA*, 17–22. Analysis of forced response of dry-friction damped structural system using an efficient hybrid frequency-time method.
18. K. Y. Sanliturk and D. J. Ewins 1996 *Journal of Sound and Vibration* **193**, 511–523. Modelling two-dimensional friction contact and its application using harmonic balance method.
19. B. D. Yang 1996 *PhD Dissertation*, *Department of Mechanical Engineering*, *The Ohio State University*. Contact kinematics of friction interfaces and applications to the prediction of resonant response of frictionally constrained turbine blades.
20. V. T. Thomson 1981 *Theory of Vibration with Applications*. Englewood Cliffs, NJ: Prentice-Hall.

APPENDIX: TRANSITION ANGLES OF SINUSOIDAL MOTION

For the sinusoidal relative motion defined in equations (22) and (23), the induced variable normal load can be described as

$$n = \begin{cases} n_0 + k_v b \sin(\theta + \phi), & \text{when } \sin(\theta + \phi) \geqslant -n_0/k_v b, \\ 0, & \text{when } \sin(\theta + \phi) < -n_0/k_v b. \end{cases} \tag{A1}$$

The transition angles at which the change of the state takes place can be derived according to the transition criteria developed in section 3.2. These transition angles will be expressed in terms of three dimensionless variables, namely $\bar{n}_0 = \mu n_0/k_u a$, $\bar{b} = \mu k_v b/k_u a$, and ϕ.

According to the criteria given by equations (13) and (16), θ_S^* and θ_*^S can be derived:

$$\theta_S^* = \theta_S^*(\bar{n}_0, \bar{b}, \phi) = \pi - \phi + \sin^{-1}(\bar{n}_0/\bar{b}), \qquad \theta_*^S = \theta_*^S(\bar{n}_0, \bar{b}, \phi) = -\phi - \sin^{-1}(\bar{n}_0/\bar{b}). \tag{A2, A3}$$

According to the criteria given by equations (14) and (15), the transition angles θ_E^P and θ_E^N can be derived:

$$\theta_E^P = \theta_E^P(\bar{b}, \phi) = \pi - \tan^{-1}\left(\frac{1 - \bar{b}\cos\phi}{\bar{b}\sin\phi}\right), \qquad \theta_E^N = \theta_E^N(\bar{b},) = \pi + \tan^{-1}\left(\frac{1 + \bar{b}\cos\phi}{\bar{b}\sin\phi}\right). \tag{A4, A5}$$

From equation (6), the friction force of the stick region from θ_E^N to ${}_N\theta_P^E$ can be expressed as

$$f = k_u(u - u(\theta_E^N)) + f(\theta_E^N). \tag{A6}$$

Since $f(\theta_E^N) = -\mu n(\theta_E^N)$, using equations (23) and (A1), equation (A6) becomes

$$f = k_u a(\sin\theta - \sin\theta_E^N) - \mu(n_0 + k_v b \sin(\theta_E^N + \phi)). \tag{A7}$$

Then, solving the criterion given by equation (11) for θ and substituting equation (A5) into the solution yield ${}_N\theta_P^E$:

$${}_N\theta_P^E = \cos^{-1}\left(\frac{\ell_2 - 2\bar{n}_0}{\ell_1}\right) - \tan^{-1}\left(\frac{1 - \bar{b}\cos\phi}{\bar{b}\sin\phi}\right), \tag{A8}$$

where ℓ_1 and ℓ_2 are defined as

$$\ell_1 = \sqrt{1 + \bar{b}^2 - 2\bar{b}\cos\phi}, \qquad \ell_2 = \sqrt{1 + \bar{b}^2 + 2\bar{b}\cos\phi}. \tag{A9}$$

Using equation (A4), equation (A8) can be simplified:

$${}_N\theta_P^E = {}_N\theta_P^E(\bar{n}_0, \bar{b}, \phi) = \pi + \theta_E^P + \cos^{-1}\left(\frac{\ell_2 - \bar{n}_0}{\ell_1}\right). \tag{A10}$$

Similar procedures can be applied to obtain ${}_S\theta_P^E$ by considering the same criterion given by equation (11), and ${}_P\theta_N^E$ and ${}_S\theta_N^E$ by considering the criterion given by equation (12):

$${}_S\theta_P^E = {}_S\theta_P^E(\bar{n}_0, \bar{b}, \phi) = \pi + \theta_E^P + \cos^{-1}\left(\frac{-\sin\theta_*^S - \bar{n}_0}{\ell_1}\right), \tag{A11}$$

$${}_P\theta_N^E = {}_P\theta_N^E(\bar{n}_0, \bar{b}, \phi) = \pi + \theta_E^N + \cos^{-1}\left(\frac{\ell_1 - 2\bar{n}_0}{\ell_2}\right), \tag{A12}$$

$${}_S\theta_N^E = {}_S\theta_N^E(\bar{n}_0, \bar{b}, \phi) = \pi + \theta_E^N + \cos^{-1}\left(\frac{\sin\theta_*^S - \bar{n}_0}{\ell_2}\right). \tag{A13}$$